UDC 621.313.33 https://doi.org/10.20998/2074-272X.2023.4.01

V.I. Milykh

Numerical-field analysis of active and reactive winding parameters and mechanical characteristics of a squirrel-cage induction motor

Introduction. *The active and reactive (inductive) winding resistances of three-phase inductions motors (IMs) are investigated. These important parameters are determined during design and are the basis for calculating a number of energy parameters and characteristics.* ***Problem.*** *In the classical design of IM, the winding resistances are determined with insufficient accuracy due to a number of assumptions and conventions. Especially it concerns the operation of IM with increased slip and it affects the accuracy of realization of its design data, starting parameters and characteristics.* ***Goal.*** *The paper aims to further develop the IM design system by numerical-field computational analysis of active and reactive resistances of the IM windings in the whole range of changes in its slip and calculation of the mechanical characteristic of IM to confirm the adequacy of the calculations of these resistances.* ***Methodology.*** *Resistances of the IM windings are determined by numerous calculations of the magnetic fields of dispersion with the FEMM program within stator and rotor teeth steps, and with current displacement in a squirrel-cage rotor core. Everything is done in the slip range when operating from start-up to idle with changing currents in the slots and the corresponding magnetic saturation of the core teeth. A Lua script has been created for the calculations, controlling the FEMM program and providing automation of all calculations.* ***Results.*** *The numerical-field method shows that the classical design method gives very large errors in determining the magnetic conductivities of IM slot dispersion, as well as current displacement in the bars of the squirrel-cage rotor winding. This is especially evident with increased slips in the start-up mode.* ***Originality.*** *Numerical estimates of the differences between the classical and numerical-field methods are given and the origin of errors is analyzed: the strong saturation of the teeth of the stator and rotor cores. This leads to a significant decrease in the magnetic conductivities of slot dispersion and the practical absence of current displacement in the rotor bars, on which the main emphasis was previously made. The obtained results made it possible to calculate the mechanical characteristic of the IM according to a transparent formula without the use of correction coefficients and reference graphical functions.* ***Practical value.*** *The provided technique of numerical-field analysis and the obtained results of the calculation of active and reactive winding resistances and mechanical characteristic are recommended as a basis for the improvement of the IM design system.* References 18, tables 7, figures 13.

Key words **induction motor, stator and rotor windings, active and reactive resistances, magnetic saturation, eddy currents, mechanical characteristics, classical design, numerical-field calculation analysis.**

Досліджуються реактивні (індуктивні) опори розсіяння і активні опори обмоток трифазних асинхронних двигунів (ТАД). Ці їхні важливі параметри визначаються при проєктуванні і є основою для розрахунку низки енергетичних параметрів та характеристик. При класичному проєктуванні ТАД опори обмоток визначаються з недостатньою точністю через низку припущень і умовностей. Особливо це стосується роботи ТАД з підвищеним ковзанням і відбивається на точності реалізації його проєктних даних, пускових параметрів та характеристик. Метою роботи є подальший розвиток системи проєктування ТАД шляхом чисельно-польового розрахункового аналізу активних і реактивних опорів обмоток ТАД у всьому діапазоні зміни його ковзання, і розрахунок механічної характеристики ТАД для підтвердження адекватності розрахунків цих опорів. Опори обмоток ТАД визначаються чисельними розрахунками магнітних полів розсіяння програмою FEMM у межах зубцевих кроків статора і ротора, а в стрижні короткозамкненого ротора – з витісненням струму. Все робиться у діапазоні ковзання при роботі від пуску до неробочого ходу зі зміною струмів в пазах і відповідного магнітного насичення зубців осердь. Для розрахунків створено скріпт Lua, який керує програмою FEMM і забезпечує автоматизацію усіх обчислень. Чисельно-польовим методом показано, що класична методика проєктування дає дуже великі похибки у визначенні магнітних провідностей пазового розсіяння ТАД, а також витіснення струму в стрижнях короткозамкненої обмотки ротора. Особливо це проявляється при підвищених ковзаннях у пусковому режимі. Надано числові оцінки розходжень класичного і чисельно-польового методів і проаналізовано походження похибок – сильне насичення зубців осердь статора і ротора. Це призводить до значного зменшення магнітних провідностей пазового розсіяння і практичної відсутності витіснення струму в стрижнях ротора, на яке раніше робився основний акцент. Отримані результати дозволили розрахувати механічну характеристику ТАД за прозорою формулою без використання коригувальних коефіцієнтів і довідникових графічних функцій. Надана методика чисельно-польового аналізу і отримані результати розрахунку опорів обмоток та механічної характеристики рекомендуються як основа для удосконалення системи проєктування ТАД. Бібл. 18, табл. 7, рис. 13.

Ключові слова: **асинхронний двигун, обмотки статора і ротора, активні і реактивні опори, магнітне насичення, вихрові струми, механічна характеристика, класичне проєктування, чисельно-польовий розрахунковий аналіз.**

Introduction. Three-phase induction motors (TIMs) are among the most common motors in various spheres of human activity. Their creation and improvement is always relevant, especially considering their diversity and mass production. This also applies to the design process with ensuring the accuracy of the implementation of design data, which allows to get rid of lengthy experimental proofs of the created samples.

Active resistances and inductive resistances of dispersion of stator and rotor windings are important parameters of the TIM, which are determined during design. They are the basis for further calculation of a number of its energy parameters and characteristics, such as operational, mechanical and starting.

For the calculation of these resistances in TIM design systems, there are established methods, set out, for example, in books [1, 2], which practically do not change for decades. In these methods, the calculation of the winding resistances at the level of the nominal load of the TIM is usually not related to fundamental problems, however, for slot, frontal and differential scattering, the

formulas of the specific magnetic conductivities are quite approximate. This is especially true for slot scattering, because different shapes of slots require separate formulas that are based on an a priori accepted simplified structure of the magnetic field.

Determination of winding resistances is significantly complicated for the operation of the TIM with increased slip in the range from the starting point to the critical point with the maximum electromagnetic torque. Here, the winding currents increase significantly and the winding resistances are affected by the saturation of the tooth structures of the stator and rotor cores, as well as the displacement of the high-frequency current in the rods of the short-circuited rotor winding.

It was recognized in [1, 2] that these phenomena primarily affect the slot dispersion of the windings and the active resistance of the rotor core, as well as the differential dispersion.

To calculate the components of the active and reactive resistances of the TIM windings that change due to the saturation of the teeth of the stator and rotor cores, the methodology of their design provides certain algorithms [1, 2]. They are built on significant assumptions, which are added to what is accepted in the calculations of the nominal load mode. For example, displacement of current in rotor slots of various shapes is based on the rectangular slots model, change of slot scattering conductivity is based on a partial reduction of its components in the upper part of the slots. And various clarifying coefficients and generalized graphic dependencies, etc. are added to everything.

Thus, the real picture of the physical phenomena taking place becomes opaque for the designer, and the results of the calculations are very approximate.

Numerical field calculations using appropriate software packages, for example, such popular ones as ANSYS Maxwell, COMSOL Multiphysics, FEMM, etc. can overcome conventions in the calculation of active and reactive resistances of TIM windings.

A large number of works, for example, [3-15] are devoted to the application of these complexes and other computational and experimental studies of parameters and characteristics of TIMs. But, fulfilling their specific purpose, they did not delve into the analysis of the active and reactive parameters of the TIM windings in the entire range of accompanying sliding. That is, they used the results of the TIM design and their created samples, without referring to the design analysis of the specified parameters. Therefore, such a task remains insufficiently studied and relevant.

The goal of the work is the further development of the TIM design system by numerical field calculation analysis of the active and reactive resistances of its windings in the range of slip s change from 1 to 0, and the calculation of the mechanical characteristics of the TIM to confirm the adequacy of the calculations of these resistances.

Analysis of the latest research. Research and use of active and inductive TIM parameters are very broad and diverse in theory, design, and experimental work.

To the already mentioned design methods [1, 2], we will add the article [3], where a numerical-field analysis of the adequacy of the design data of the TIM and a method of their refinement are proposed, which also required the use of the specified parameters.

The work [4] is interesting, where it is emphasized that in order to control and achieve an effective TIM drive, a deep understanding and accurate determination of its parametric characteristics is necessary. Accordingly, a critical analysis of modern methods of their determination is carried out, and based on the T-shaped replacement circuit of TIM, an effective method is proposed, which consists of a test without a rotor and with a double load. In-depth experiments on the study of active resistances and inductances of the windings are performed depending on the stator current and frequency. It is noted that the effect of magnetic saturation, losses in the core and skin effect in the rotor rod is fully taken into account, which ensures the accuracy of the measurement of TIM parameters.

In the practice of calculating parameters and characteristics of TIMs, the evolution took place depending on the availability of technical capabilities and software.

The article [5] is devoted to determining the parameters of the TIM replacement circuit according to the passport data of induction motors and constructing their mechanical characteristics with an analysis of the calculation error. Variants of refinement of the well-known Kloss formula and a modified critical slip formula are considered. But it is not talking about changes in TIM parameters due to saturation of the magnetic core and displacement of current in the rotor winding.

Inductances of stator and rotor windings and magnetic scattering in [6] are determined by the Finite Element Method. The studies are carried out when the magnetizing currents and rotor speed change and reflect the change in TIM parameters. But they are determined for windings as a whole without analysis of components of inductances and current displacement in the rotor rods.

In [7], the parameters of the TIM with a complicated stator winding are also determined by numerical field analysis to prove the improvement of the harmonic composition and performance of the machine. The basis of the analysis is a T-shaped TIM replacement circuit, the parameters of which are based on generally accepted assumptions.

In [8], a 3D mathematical model of transient electromagnetic fields was developed to identify the active and inductive resistances of a short-circuit of the TIM, which takes into account the nonlinearity of the electrophysical and magnetic properties of materials.

In [9], the equation obtained for determining the active resistance of the stator phase winding, which consists of the relationship of the average values of the integral functions of the current and voltage in the steady state mode of operation is considered, which is focused on the analysis of the parametric asymmetry of the induction motor.

In [10], an overview of identification methods for obtaining accurate parameters of an induction motor

offline and online, taking into account the increase in winding temperature, skin effect and saturation of the magnetic core, is provided. During identification, the motor is kept at a standstill and a DC voltage or single-phase AC voltage signal is applied.

The article [11] presents an induction motor parameter estimator based on the model reference adaptive system (MRAS). A new concept of the PQ-MRAS estimator is proposed, which allows simultaneous calculation of the stator and rotor resistances, which is considered its main advantage. The estimator uses the active and reactive powers of the machine, which are calculated from the single measured stator voltage and current.

In [12, 13], an algorithm for calculating mechanical characteristics and methods for analyzing starting modes of induction motors with a short-circuited rotor are proposed. The developed calculation methods are based on a mathematical model of TIM, which takes into account the change in own and mutual differential inductive resistance due to the saturation of the magnetic core and the active resistance of the rotor winding due to the displacement of the current in its rods. However, the actual active and inductive resistances as such are not provided and not analyzed.

The article [14] presents a new methodology for measuring the resistance of an induction motor for mass production, and analyzes the dependence of the inductance of its winding on the magnetizing current and higher-order voltage harmonics, and also provides a simulation model of the motor's resistance to their influence.

In [15] adaptive modeling of TIM is discussed for the purpose of its refined design and compliance with protection standards and a specific purpose. An algorithm for the implementation of static and dynamic simulation of an induction machine is provided, which is verified on the basis of several common methods. One of the foundations of modeling is the T-shaped substitution circuit in various variations of its structure and parameters.

Object of study. To demonstrate the ongoing research, a TIM variant with nominal power P_N = 15 kW; phase voltage U_{sN} = 220 V and frequency f_s = 50 Hz; number of phases m_s = 3 and number of pairs of poles p = 2 was adopted. According to the design calculation of this TIM, in [2] the following was determined: the height of the axis of rotation h = 160 mm, the outer diameters of the stator d_{se} = 0.272 m and the rotor d_r = 0.184 m; air gap δ = 0.5 mm; nominal slip s_N = 0.0026; active length l_a = 0.13 m; rated stator phase current I_{sN} = 29 A; the number of its slots Q_s = 48 and consecutive turns on the phase winding N_s = 112, the number of parallel branches a_s = 2, the winding coefficient K_{Ws} = 0.959; rotor phase current I_{rN} = 442 A; the number of slots Q_r = 38.

The stator winding is single-layer, diametrical, which is typical for TIM of certain power. The rotor winding is short-circuited cast of an aluminum alloy, there is no bevel of the slots, therefore the bevel coefficient K_{sqr} = 1.

The general layout of the TIM is given in Fig. 1.

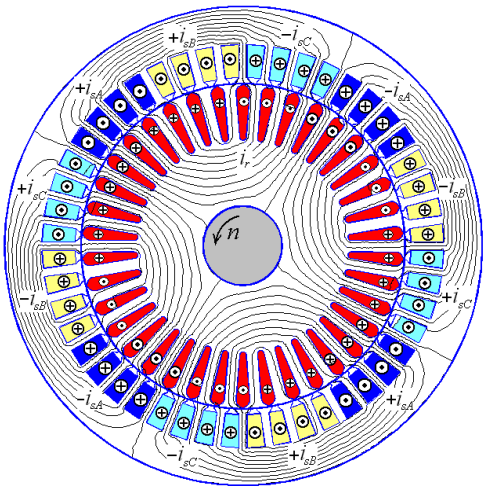

Fig. 1. TIM electromagnetic system with the distribution of currents in its windings and the picture of the lines of force of the magnetic field at nominal load

In this TIM, common shapes of stator and rotor slots of general industrial TIMs [1, 2] are used, which are shown in Fig. 2 together with teeth and size designation (in mm). The rotor core is complicated by a jumper of thickness h_{r0}, which makes the slot closed.

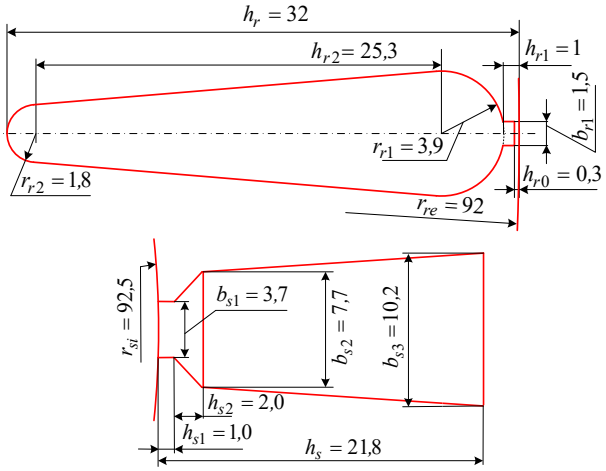

Fig. 2. Slots of the rotor and stator of the considered TIM

Specific formulas of the specific magnetic conductivities of slot scattering correspond to the specific shapes of the slots in the classical method of TIM calculations. But this does not complicate numerical field calculations of magnetic fields, because they are universal and the calculation algorithm does not change when changing from one shape of slot to another. The same applies also to the calculation of the current distribution in the slots of the rotor, taking into account the effect of its displacement.

Fundamentals of numerical-field electromagnetic calculations. Magnetic fields in the TIM are calculated using the well-known Finite Element Method in the popular FEMM software package [16]. Since many calculation options were planned, the process of designing the TIM, building its physical and geometric model in the FEMM software environment, control of magnetic field calculations and determination of the necessary electromagnetic parameters were automated. For this

purpose, following the example in [17] and other author's works, a script was created in the algorithmic language Lua, integrated into the FEMM program.

The stationary magnetic field of the TIM in its central cross-section is described by a well-known 2D differential equation [16]:

$$\mathrm{rot}[\mu_a^{-1}\mathrm{rot}(\vec{k}A_z)] = \vec{k}J_z\,, \qquad (1)$$

where A_z, J_z are the axial components of the magnetic vector potential (MVP) and current density; μ_a is the absolute magnetic permeability; $\vec{k}$ is the ort along the axial axis z.

The propagation of the magnetic field is limited by the outer surface of the stator core, where the Dirichlet boundary condition is set for the MVP: $A_z = 0$. Figure 1 provides an example of a picture of the lines of force of the magnetic field of the TIM at the nominal load.

When calculating the magnetic field together with the eddy currents in the rotor slots, the formulation of the problem changes. In this case, the FEMM program solves the harmonic problem of a plane-parallel electromagnetic field based on the solution of the equation [16]:

$$\mathrm{rot}[\mu_a^{-1}\,\mathrm{rot}(\vec{k}A_z)] = \vec{k}(J_{z\,st} - \gamma_{Al}\frac{\partial A_z}{\partial t})\,, \qquad (2)$$

where A_z, $J_{z\,st}$, $J_{z\,ec} = -\gamma_{Al}\dfrac{\partial A_z}{\partial t}$ are the values of MVP and density of external and eddy currents that change in space and time; γ_{Al} is the specific electrical conductivity of the rotor bar material.

Now, in the complicated case of the mathematical model (2), the axial component of the current density has two components:

$$J_z = J_{z\,st} + J_{z\,ec}\,. \qquad (3)$$

Note that when solving equation (2), the FEMM program operates with complex values that reflect harmonic electromagnetic quantities that change with the frequency of the external current. The calculation results are outputted in the same form, i.e. in their complex values.

To determine a sufficient zone for calculating the distribution of currents in the rotor slots, test calculations were previously performed.

From the considered variants of the electromagnetic field modeling zone, the full geometric model of the TIM, which is shown in Fig. 1, is first selected.

When calculating the current distribution in the rotor winding rods, two rotor winding rods in diametrically located slots are designated as active. The currents in them are directed oppositely to ensure their asymmetry and zero balance of the total current in the calculation zone. There were no currents in the remaining slots of the rotor and stator. The frequency of change of the rotor currents in the start-up mode for the FEMM program is set as $f_r = f_s$.

For the rods in the slots of the rotor, the electrical conductivity of the aluminum casting in the cold state is adopted $\gamma_{Al} = 27$ MS/m [1]. It was found that in both slots the current density distribution was the same with a change of sign.

After preliminary calculations, another calculation model was applied, which is shown in Fig. 3. This is, in fact, a fragment of the complete model in Fig. 1, but within the tooth pitch of the rotor with the capture of the back part of the rotor core and the air gap with the conventional part of the adjacent stator core. Calculations of the magnetic field with eddy currents on this model gave almost the same results as in the previous case. This corresponds to what is done when determining inductive parameters and current displacement in TIM design methods. Moreover, there the calculation zone is limited only to the slot without involving the adjacent parts of the tooth zone, for which the magnetic permeability is considered infinitely large.

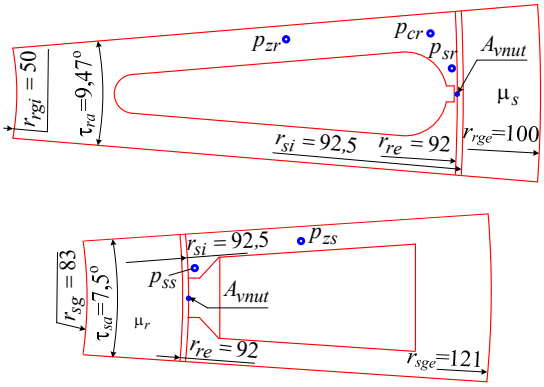

Fig. 3. Calculation models of rotor and stator slots within their tooth pitches

Similarly, the zone of magnetic field calculation is also adopted for the stator slot – it is also shown in Fig. 3 and captures the g slot pitch of the stator core with adjacent parts of its teeth and back, as well as the gap and conventional part of the rotor core.

Thus, when calculating magnetic fields, the calculation models shown in Fig. 3 are used: for the stator slot – according to (1), for the rotor slot – according to (2) taking into account eddy currents.

Since in both cases the magnetic field of slot scattering is calculated, it is considered that beyond the outer limits of the calculation models in Fig. 3 it does not propagate. Therefore, the already mentioned Dirichlet boundary condition is set here for the MVP: $A_z = 0$.

When calculating the magnetic field of the rotor slot, the magnetic properties of the adjacent part of its core were set by the magnetization curve of the corresponding steel, and the constant magnetic permeability μ_s was set for the conventional part of the stator core. When calculating the magnetic field of the stator slot, it was done similarly, and in the conditional part of the rotor core, a constant magnetic permeability μ_r was set. This is indicated in Fig. 3, and below μ_s and μ_r are the relative magnetic permeabilities and their values are given in relative units (p.u.).

Solution of (1), (2) for the FEMM program is a trivial task. Here, external currents are set in the slots, and as a result of the numerical calculation, the program provides the distribution of MVP, and for the rotor slot, the distribution of eddy currents.

After that, it is time to determine the magnetic conductivities of the slot dispersion of the conductors and

the active resistance of the rotor rod. Let's consider the method of this on the example of the rotor slot, for the magnetic conductivities of the stator slot it works similarly.

Examples of pictures of the calculated magnetic fields for the slots of the rotor and stator are given in Fig. 4 (so far without eddy currents in the rotor slot).

For the slot of the rotor or stator, a single (for one conductor) magnetic flux linkage (MFL) is determined together with the «ballast», which is provided by the magnetic field that goes into the gap and the core behind it, Wb:

$$\Psi_{nut} = \frac{1}{S_{nut}} \int_{S_{nut}} A_z dS , \qquad (4)$$

where S_{nut} is the area of the conductor part of the sot, m^2.

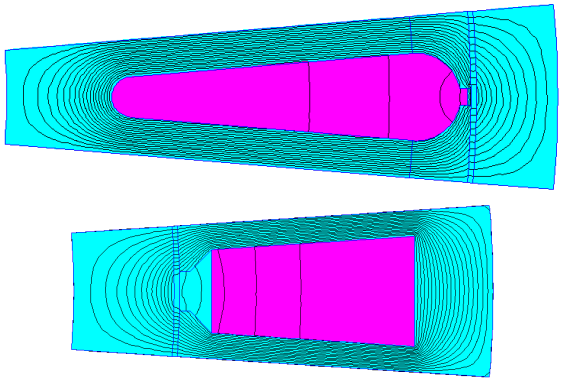

Fig. 4. Pictures of the magnetic field of the rotor bar at μ_s =1000 and stator at μ_r =1000 and nominal currents

MFL of scattering of the inner part of the slot, Wb:

$$\Psi_{rn} = \Psi_{nut} - \Phi_{vnut}, \qquad (5)$$

where Φ_{vnut} is the magnetic flux behind the slot spline (ballast), Wb:

$$\Phi_{vnut} = A_{vnut} \cdot l_a, \qquad (6)$$

where A_{vnut} is the value of MVP, Wb/m, on the surface in the upper part of the slots – at the points given in Fig. 3.

According to MFL (5), the unit inductance of the slot dispersion of conductors in the slot, H, is determined:

$$L_{\sigma rn} = \Psi_{rn} / I_{nut}, \qquad (7)$$

where I_{nut} is the amplitude of the external current, A, in the slot: for the rotor $I_{nut} = \sqrt{2} I_r$ (without eddy currents, which ultimately give a zero contribution); for the stator $I_{nut} = z_{Qs} \sqrt{2} I_s$, where I_r, I_s are the effective values of the currents; z_{Qs} is the number of effective conductors in the stator slot.

The main result is the desired specific magnetic conductivity of the scattering of the inner part of the slot, i.e.:

$$\lambda_{rn} = L_{\sigma rn} / (\mu_0 l_a), \qquad (8)$$

where μ_0 is the magnetic constant ($\mu_0 = 4 \cdot \pi \cdot 10^{-7}$ H/m).

To determine the active resistance of the rotor rod, taking into account the nonuniform distribution of the current density in it, the following steps are carried out.

According to the found distribution of the current density J_z, the active power losses in the rotor core, W, are directly determined by the FEMM program:

$$P_{nr} = \frac{l_a}{\gamma_{Al}} \int_{S_{nut}} J_z^2 dS . \qquad (9)$$

Then the desired active resistance of the rotor winding rod, taking into account the displacement of the current in it, Ω:

$$R_{nr} = 2 \cdot P_{nr} / I_{nut}^2 . \qquad (10)$$

With uniform current distribution, the active resistance of the rotor rod, Ω:

$$R_{nr0} = \frac{l_a}{\gamma_{Al} S_{nut}} . \qquad (11)$$

The degree of change in resistance of the rotor rod is estimated by the coefficient of displacement of its current

$$k_{Rr} = R_{nr} / R_{nr0} . \qquad (12)$$

Analysis of the results of calculations of magnetic fields, eddy currents and parameters of conductors in the slots of the rotor and stator. The main part of the calculations was performed based on the working temperature of the TIM windings, which in the project according to [2] is equal to 115 °C. Here, the specific electrical conductivity of aluminum casting $\gamma_{Al115\ C}$ for the rods of the rotor winding is taken to be equal to 20.5 MS/m.

In order to have basic points of reference, we will give the values of TIM parameters from the project [2]: the magnetic conductivities of the slot dispersion of the rotor λ_{rnb} = 2.64 and the stator λ_{snb} = 1.48, the cross-sectional area of the rotor winding rod S_{rc} = 173.2 mm^2 and its active resistance $R_{nr0} = 34.2 \cdot 10^{-6}$ Ω at temperature of 115 °C.

Considering different calculation modes, the currents in the slots of the rotor and stator (Fig. 3) will be given in relative units (p.u.) as their multiples relative to the nominal values I_{rN} and I_{sN}:

$$k_{Ir} = I_r / I_{rN} ; \quad k_{Is} = I_s / I_{sN}. \qquad (13)$$

To enter the calculations of the magnetic field and parameters at a clear level, let's start with the nominal mode with k_{Ir} = 1, k_{Is} = 1 and the corresponding slip s_N. We will perform the first calculations with unsaturated inactive parts of the calculation models in Fig. 3, for which it is sufficient to take μ_s = 1000 or μ_r = 1000.

The results of the numerical-field calculation of magnetic flux linkages and inductive parameters according to (4)–(8) for the rotor core are given in Table 1, for stator conductors – in Table 2 (in the first rows of the tables), and the pictures of the magnetic fields are already shown in Fig. 4.

Table 1

MFL and inductive parameters of the rotor core at $s = s_N$; k_{Ir} =1; f_r = 1.3 Hz

μ_s, p.u.	Ψ_{nut}, 10^{-4} Wb	A_{vnut}, 10^{-3} Wb/m	Φ_{vnut}, 10^{-4} Wb	Ψ_{rn}, 10^{-4} Wb	$L_{\sigma rn}$, 10^{-7} H	λ_{rn}, p.u.
1000	8,982	4,511	5,864	3,119	4,989	3,054
50	8,400	3,985	5,180	3,220	5,152	3,154
1	4,280	0,6622	0,8609	3,419	5,469	3,348
0,01	3,621	0,1591	0,2068	3,414	5,462	3,343

Table 2

MFL and inductive parameters of stator winding conductors at k_{Is} =1; f_s = 50 Hz

μ_r, p.u..	Ψ_{nut}, 10^{-4} Wb	A_{vnut}, 10^{-3} Wb/m	Φ_{vnut}, 10^{-4} Wb	Ψ_{sn}, 10^{-4} Wb	$L_{\sigma sn}$, 10^{-7} H	λ_{sn}, p.u.
1000	5,41	2,96	3,85	1,562	2,721	1,665
50	4,96	2,62	3,40	1,562	2,720	1,665
1	2,02	0,42	0,556	1,471	2,561	1,568
0,01	1,52	0,070	0,0904	1,431	2,492	1,526

For the main parameter – the magnetic conductivity of slot scattering, the numerical field calculation gave results that exceed the data of classical calculations for rotor and stator slots by 15.7 and 12.5 %. Due to the low frequency of the rotor current f_r = 1.3 Hz, the influence of eddy currents is practically absent.

It can be assumed that the increase in magnetic conductivities was due to a more natural structure of the lines of force of the magnetic field in the upper parts of the slots, where their density and, accordingly, their role is the most significant, while the classical technique is a priori based on an overly simplified structure of the lines of force.

Let us analyze in more detail the structure of the magnetic conductivity of the rotor slot in its upper part – in the jumper zone, which is shown in Fig. 2, 5.

Magnetic conductivity of the slot on the thickness of the jumper according to the conditional formula from the design methodology [2]

$$\lambda_{rnh0} = \frac{1{,}12 \cdot h_{r0}}{I_{rN}} \cdot 10^{-3} = 0{,}760, \qquad (14)$$

and it is also through a numerical field calculation:

$$\lambda_{rnh0\mu} = \frac{A_{nnut} - A_{vnut}}{\mu_0 I_{nut}} = 1{,}243. \qquad (15)$$

where A_{nnut}, A_{vnut} are the values of MVP at the lower and upper points of the jumper, which are indicated in Fig. 5.

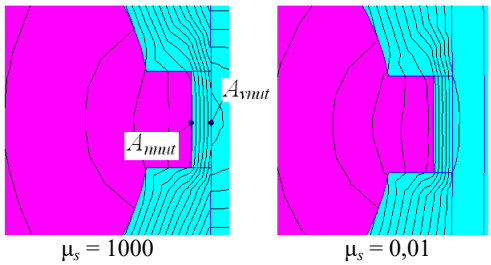

Fig. 5. Fragment of the rotor slot in its upper part

It can be seen that the difference is very large and amounts to 63.5 %, although in the full value of the magnetic conductivity of the dispersion of the rotor slot it looks like 15.9 %. Here, the magnetic flux density in the middle of the jumper is 3.28 T, and the relative magnetic permeability is 12.

It is interesting that if there were no jumper, then this very place, but non-magnetic, would give magnetic conductivity

$$\lambda_{rnh0} = \frac{h_{r0}}{b_{r1}} = 0{,}20, \qquad (16)$$

that is, the steel jumper of the slot significantly increases the value of the inductive parameters of the rotor winding.

In the absence of current displacement in the rotor slot, the active resistance of the rod according to (10) $R_{nr} = 36.2 \cdot 10^{-6}$ Ω, which is slightly different from the design value R_{nr0} given above. This is due to the fact that the FEMM program by its means determines the cross-sectional area of the rotor winding rod more accurately: S_{nut} = 175.1 mm^2.

On the calculation models in Fig. 3, it was checked how the value of the magnetic conductivity of the inactive part of the calculation zones affects the calculation results. For this, to the already used values μ_s = 1000 and μ_r = 1000 we also added values of 50, 1, and 0.01.

The resulting pictures of the lines of force of the magnetic field are given for the rotor slot in Fig. 6, for the stator slot – in Fig. 7, and the results of the calculations are placed in the next rows of the same Tables 1, 2.

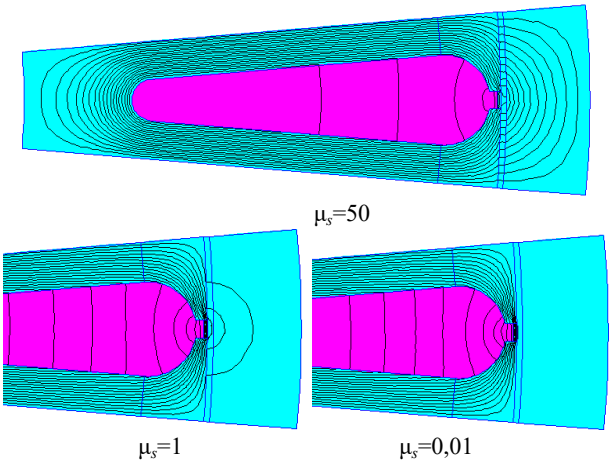

Fig. 6. Pictures of the magnetic field of the rotor rod at different values of the magnetic permeability of the stator core zone

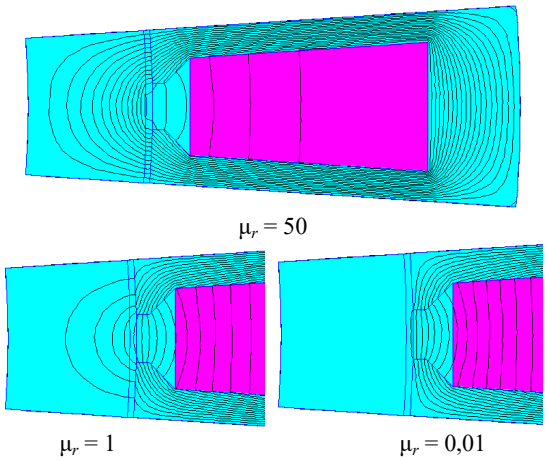

Fig. 7. Pictures of the magnetic field of the stator slot at different values of the magnetic permeability of the rotor core zone

Naturally, as the magnetic permeability of the inactive part decreases, a smaller fraction of the magnetic field passes through the gap, and in the extreme case, at μ_s = 0.01 and μ_r = 0.01, this path is almost completely closed. This just corresponds to the usual assumption when considering slot scattering in [1, 2].

But in other versions, formula (5) singles out exactly the inner slot part of the magnetic field, therefore, in

Tables 1, 2 the conductivity values change relatively weakly. Although there are changes, and this means that there is still some redistribution of the magnetic field. But all the same, the values of λ_{rn} and λ_{rn} turn out to be larger, compared to the basic values from the design calculation.

In classical TIM design, it is considered that the effect of current displacement in the rods of the rotor winding is most pronounced at the initial moment of starting when slip s = 1. Moreover, the current distribution is initially determined by analytically solving the equation of the electromagnetic field for a rectangular slot with unsaturated core teeth. Then, for specific shapes of the slot, the result of calculating the active resistance of the winding rod is adjusted on the basis of reference dependencies and correction coefficients formed based on the experience of TIM design. The slot scattering magnetic conductivities obtained for the nominal mode are also corrected in a similar way, and here the saturation of the teeth is indirectly taken into account. It is clear that there is not enough specific physics of the process here, and as a result, a lot of errors in the calculation of the starting parameters accumulate.

Numerical-field calculations are able to bring clarity to this issue and clarify the results, because here conventions and assumptions are made much less, although it is impossible to completely do without them, considering the complexity of the process.

So, let's start as in the classical design, considering the eddy currents in the rotor slot with unsaturated teeth at the multiplicity of the rotor current k_{Ir} = 1, but with the slip s = 1 and the frequency f_r = 50 Hz.

The resulting toned picture of the current density distribution in the rotor slot is given in Fig. 8, where its increase in the upper part of the slot is visible. This is confirmed in Fig. 9, which shows the graphs of the distribution of the current density on the line of symmetry of the Flot by its height. Here there are three options from the complex value of the density of the combined external J_{st} and eddy J_{ec} currents: $|J_{st} + J_{ec}|$ – module; $\mathrm{Re}|J_{st} + J_{ec}|$ – real and $\mathrm{Im}|J_{st} + J_{ec}|$ – imaginary components.

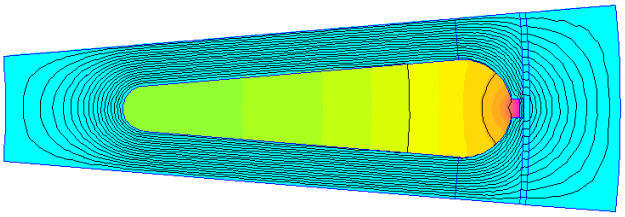

Fig. 8. Picture of the magnetic field of the rotor rod at nonuniform distribution of its current (f_r = 50 Hz, μ_s =1000)

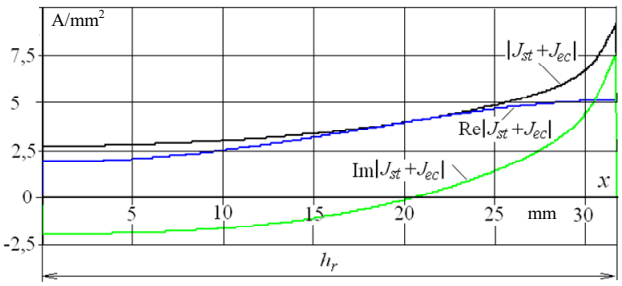

Fig. 9. Distributions of current density components by the height of the rotor slot

A number of calculation results obtained by (8) – (10), (12) are given in Table 3.

Table 3

Data of calculating the parameters of the rotor rod and conductors in the slot of the TIM stator at f_r = 50 Hz and k_{Ir} =1, k_{Ii} =1

μ_s, p.u.	P_{nr}, W	R_{nr} μΩ	k_{Rr}	J_{rmax}, A/mm²	J_{rmin}, A/mm²	λ_{rn} p.u.	μ_r, p.u.	λ_{sn} p.u.
1000	9,6	49,0	1,352	5,08	1,85	2,907	1000	1,665
50	9,9	50,6	1,398	5,19	1,73	2,989	50	1,665
1	10,65	54,5	1,506	5,42	1,45	3,133	1	1,568
0,01	10,7	54,8	1,513	5,43	1,43	3,126	0,01	1,526

In numerical form, the nonuniformity of the current density distribution is revealed by the difference in the real component of the current density in the upper J_{rmax} and lower J_{rmin} points of the slot. This is the algebraic sum of the density of external J_{st} and eddy J_{ec} currents. The FEMM program provides output of such data, and they are at μ_s = 1000 in the first line of the Table 3. Naturally, the J_{st} component throughout the slot is constant and equal to 4.83 A/mm², and J_{ec} varies from top to bottom from 0.26 to –2.98 A/mm².

Note that at μ_s = 1000 in this control test version, a noticeable displacement of the current into the upper part of the slot and a corresponding increase in the active resistance of the rod by 1.35 times are manifested, as evidenced by the current displacement coefficient k_{Rr}.

It is also interesting that the specific magnetic conductivity of the rotor slot λ_{rn} compared to the data in Table 1 (without current displacement) decreased by 4.8 %, and the magnetic conductivity of the stator slot λ_{sn} is not related to this.

What was done in the presented calculation at μ_s = 1000 was repeated at other values of the magnetic permeability of the stator core, as it was in Table 1. It can be seen that even when taking into account the displacement of the current with a decrease in μ_s, the coefficient of displacement of the current in the rotor core and the magnetic conductivity λ_{rn} increase. That is, for λ_{rn}, the same happens as in the absence of current displacement, but in the new variant, the values of λ_{rn} turn out to be somewhat smaller.

The performed calculations showed such a level of displacement of the rotor current, which is usually used in the classical design of the TIM. But in these demonstration calculations, the nominal current of the rotor core was artificially accepted, and accordingly the teeth of the rotor core were not saturated (except for the jumper). The value of magnetic flux density and relative magnetic permeability of the rotor tooth at the control points marked in Fig. 3, are given in Table 4 with the specified options for μ_s.

Table 4

Magnetic flux density and magnetic permeability in the rotor teeth at s = 1 and k_{Ir} = 1

μ_s, p.u.	Rotor tooth							
	Jumper		Crown		Schlitz		Leg	
	B_{rh0}	μ_{rh0}	B_{rc}	μ_{rc}	B_{rs}	μ_{rs}	B_{rz}	μ_{rz}
1000	3,28	12	1,63	1982	1,91	1587	2,19	1068
50	3,30	11	1,50	2137	1,89	1624	2,04	1347
0,01	3,45	8	0,52	2508	1,26	2323	0,87	2435

To increase the level of adequacy, further calculations are performed taking into account realistic values of the currents in the slots of the rotor and stator, which correspond to the start of the TIM. According to the slip s = 1, the frequency of the rotor current is f_r = 50 Hz, and the multiples of the currents are taken according to the TIM project from [2], according to which at the initial moment of start-up k_{Ir} = 6.33 and k_{Is} = 5.84. Here, as in the previous calculations, a number of relative magnetic permeability values μ_s and μ_r are taken for the inactive parts of the models shown in Fig. 3.

The calculation results are given in Table 5 – they are determined by (9), (10), (12) and (8), as well as the current density in the upper and lower points of the rotor slot is given (average value J_{st} = 22.6 A/mm^2).

The saturation level of the rotor and stator teeth is characterized by the data in Tables 6, 7, where the values of magnetic flux density and relative magnetic permeability at the points marked in Fig. 3 are given.

Table 5

Parameters of the rotor rod and conductors of the TIM stator slot at f_r = 50 Hz, k_{Ir} = 6.33 and k_{Is} = 5.84

μ_s, p.u.	P_{nr}, W	R_{nr} μΩ	k_{Rr}	J_{rmax}, A/mm^2	J_{rmin}, A/mm^2	λ_{rn} p.u.	μ_r, p.u.	λ_{sn} p.u.
1000	284	36,28	1,002	23,0	22,6	0,501	1000	0,435
50	284	36,32	1,003	23,1	22,3	0,555	50	0,476
1	314	40,20	1,110	26,3	18,4	1,260	1	1,092
0,01	342	43,72	1,208	28,0	16,2	1,508	0,01	1,305

Data in Table 4, 6, 7 show that when going from the unsaturated magnetic state at k_{Ir} = 1 and k_{Is} = 1 to the highly saturated state at k_{Ir} = 6.33 and k_{Is} = 5.84, the magnetic flux density increased significantly, and the magnetic permeability decreased accordingly.

Table 6

Magnetic flux density and magnetic permeability in the rotor teeth at s = 1, k_{Ir} = 6.33 and k_{Is} = 5.84

μ_s, p.u.	Rotor tooth							
	Jumper		Crown		Schlitz		Leg	
	B_{rh0}	μ_{rh0}	B_{rc}	μ_{rc}	B_{rs}	μ_{rs}	B_{rz}	μ_{rz}
1	4,32	3	1,83	1701	3,18	17	2,94	99
50	3,5	7	2,45	583	2,79	191	3,06	38

Due to the change in saturation, there were significant changes in the electromagnetic parameters in the slots of the rotor and stator, as evidenced by the comparison of the data in Tables 1, 2, 3, 5.

Table 7

Magnetic flux density and magnetic permeability in the rotor teeth at s = 1 as well as different k_{Ir} and k_{Is}

μ_r, p.u.	k_{Ir} / k_{Ir}, p.u.	Rotor tooth			
		Schlitz		Leg	
		B_{ss}	μ_{ss}	B_{sz}	μ_{sz}
1	6,33 / 5,84	1,62	1998	2,78	196
50	6,33 / 5,84	1,67	1939	3,06	39
50	1 / 1	0,85	2437	1,64	1975
1000	1 / 1	0,92	2433	1,79	1768

The coefficient of current displacement in the rotor rod k_{Rr} significantly decreased, especially in the options μ_s = 50 (the most realistic) and μ_s = 1000. The same happened with the magnetic conductivities of slot scattering λ_{rn} and λ_{sn}, which at μ_s = 50 and μ_r = 50 decreased by 5.49 and 3.5 times respectively. It can be imagined that for the characteristics of the TIM, this will have a more significant impact than changes in the active resistance of the rotor rods, which is usually the focus of attention during their classical design. Moreover, as can be seen from the Table 5, displacement of the current in the rotor bar is practically not manifested.

Mechanical characteristics of TIM. In order to bring all the active and reactive resistances of the TIM windings together and see their realism, their adequacy was checked using the calculation and analysis of the mechanical characteristic $M_{em}(s)$ – the dependence of the electromagnetic torque on slip in the range of its change from 0 to 1.

When calculating the electromagnetic torque, the well-known formula from the TIM theory is used:

$$M_{em} = \frac{pm_s U_s^2 \frac{R_r'}{s}}{\omega_s \left[\left(R_s + C_{\sigma s} \frac{R_r'}{s} \right)^2 + \left(X_{\sigma s} + C_{\sigma s} X_{\sigma r}' \right)^2 \right]}. \quad (17)$$

The following algorithm is used to calculate the parameters of TIM windings by analogy with [1, 2].

Active resistance of the rotor winding

$$R_r = R_{nr} + R_{r\,fr}, \quad (18)$$

where R_{nr} is the resistance of the rod, which is determined by (10); R_{rfr} s the resistance of the short-circuited rings reduced to the rod current.

The inductive resistance of the dispersion of the phase winding of the stator

$$X_{\sigma s} = 1{,}58 \cdot \frac{f_s \cdot l_a \cdot N_s^2 \cdot \lambda_{\sigma s}}{p \cdot q_s \cdot 10^5}, \quad (19)$$

where its total coefficient of scattering conductivity

$$\lambda_{\sigma s} = \lambda_{s n} + \lambda_{s d} + \lambda_{s fh} \quad (20)$$

consists of the coefficients of scattering conductivity of slot $\lambda_{s n}$, differential $\lambda_{s d}$ and frontal $\lambda_{s fh}$.

Inductive resistance of the rotor winding

$$X_{\sigma r} = 7{,}9 \cdot f_s \cdot l_a \cdot \lambda_{\sigma r} \cdot 10^{-6}, \quad (21)$$

where its total coefficient of scattering conductivity

$$\lambda_{\sigma r} = \lambda_{r n} + \lambda_{r d} + \lambda_{r fh} + \lambda_{r sq} \quad (22)$$

consists of the coefficients of scattering conductivity of slot $\lambda_{r n}$, differential $\lambda_{r d}$ and short-circuited rings $\lambda_{r fh}$ ($\lambda_{r sq}$ – the coefficient of dissipation of slot bevel in this case is absent due to the absence of a bevel).

Formula (17) includes the active and inductive resistances of the rotor winding reduced to the stator winding

$$R_r' = K_{sr} R_r; \; X_{\sigma r}' = K_{sr} \cdot X_{\sigma r}, \quad (23)$$

where K_{sr} is the reducing factor.

Among the values that provide (17) according to numerical-field calculations, R_{nr}, $\lambda_{s\ n}$, $\lambda_{r\ n}$ and values dependent on them change.

Differential conductivities, according to [2], also depend on the saturation of the teeth of the cores, but

specific formulas and recommendations are not provided, which requires separate studies. Therefore, in order to reflect the fact of dependence, conventional formulas for the saturated differential conductivities of the stator and rotor are adopted:

$$\lambda_{s\,d} = k_{sd\mu}\lambda_{s\,db}\,;\quad \lambda_{rd} = k_{rd\mu}\lambda_{r\,db}\,, \qquad (24)$$

where are the current-dependent reduction factors

$$k_{sd\mu} = 1 + \frac{(k_{d\mu}-1)(k_{Is}-1)}{(k_{Is1}-1)}\,;\; k_{rd\mu} = 1 + \frac{(k_{d\mu}-1)(k_{Ir}-1)}{(k_{Ir1}-1)}\,,$$

in which $\lambda_{s\,db}$, $\lambda_{r\,db}$ are the base values of conductivities in the unsaturated state (s –> 0); k_{Is1}, k_{Ir1} are the multiples of currents at s = 1; $k_{d\mu}$ is the multiplicity of the differential conductivity at s = 1 relative to the base value at s = 0, which was taken to be equal to 0.7 (in reality it may be less, taking into account the detected changes in slot conductivities). The decrease in differential conductivities is explained by the «smoothing out» of the magnetic inhomogeneity of the tooth-slot structures with strong saturation of their teeth. This issue can be considered separately by analyzing the harmonic composition of the EMF of the windings on the basis of, for example, that presented in [18].

A number of values from (17) – (23) are considered independent of the slip and saturation of the teeth of the cores, and they are accepted according to the project, namely: $R_{r\,fh}$ = 16.2·10^{-6} Ω; R_s = 0.402 Ω; $\lambda_{s\,db}$ = 1.57; $\lambda_{r\,db}$ = 2.08; $\lambda_{s\,fh}$ = 1.45 and $\lambda_{r\,fh}$ = 0.61; K_{sr} = 3636 (the last four are in p.u.).

According to the design calculation of the TIM, the following are also determined: $C_{\sigma s}$ = 1 + $k_{\sigma s}$ is the coefficient of the magnetic circuit for the stator winding, where $k_{\sigma s} = X_{\sigma s} / X_{\mu}$ is its dispersion coefficient; X_{μ} is the main inductive resistance; $\omega_s = 2\pi f_s$ = 314 s^{-1} is the angular frequency of the stator current.

As a result, the dimensionless coefficient $C_{\sigma s}$ varied from 1.018 to 1.027 when the slip changed from 1 to 0.

When calculating the mechanical characteristics according to (17) when the slip s changes, the multiples of the currents of the stator and rotor windings k_{Ir} and k_{Is} were determined according to the design method [2]: their dependence on s in graphic form is given in Fig. 10.

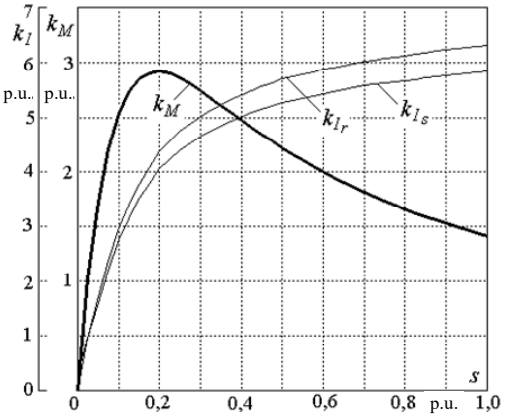

Fig. 10. Dependence of rotor and stator currents on slip and mechanical characteristics of TIM

Calculating each point of this characteristic according to the models in Fig. 3, for inactive parts, that is, parts of the stator and rotor cores, the relative magnetic permeabilities μ_s and μ_r were taken to be equal to 50. Considering the data in the tables, this level corresponds to the saturated state of the teeth, but gives stable results for points with reduced saturation.

A set of parameters for this calculation option for the starting point at s = 1, k_{Ir} = 6.33 and k_{Is} = 5.84 is provided in Tables 5 – 7. The patterns of the magnetic field in the slots of the rotor and stator are shown in Fig. 11, where it can be seen that displacement of the current of the rotor rod actually does not occur: this can be explained in the case of small slips by the low frequency of the current, and in the case of large slips by the strong saturation of the teeth. Note that the detected absence of current displacement in the rotor rods in the start-up mode contradicts the classics, which is news!

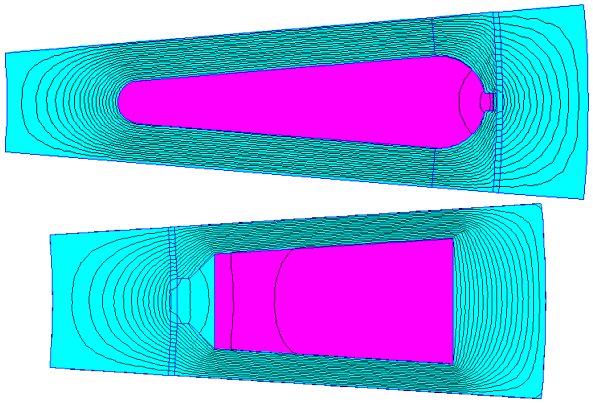

Fig. 11. Pictures of the magnetic field in the slots of the rotor and stator of the calculated version for the starting point

The actual mechanical characteristics in a dimensionless form are shown in Fig. 10, where k_M is the multiple of the torque relative to its nominal value.

According to the calculation of the mechanical characteristics, it was found that the nominal electromagnetic torque 102 N·m; when slip s = 1, the multiplicity of the starting torque k_{M1} = 1.41; overload capacity k_{Mm} = 2.93 at critical slip s_{cr} = 0.20. Note that in the project according to [2], the values of similar quantities were as follows: M_{emN} = 99.4 N·m; k_{M1} = 1.44; k_{Mm} = 2.5 at s_{cr} = 0.15.

But it is also possible to compare the data of the calculated mechanical characteristics of a serial four-pole TIM type AIR160S4 with similar parameters: P_N =15 kW; h = 160 mm; I_{sN} = 29.0 A; k_{I1} = 7; k_{M1} = 1.9; k_{Mm} = 2.9; M_N = 98.1 N·m (nominal torque on the shaft). Then we can verify the adequacy of the given numerical-field method of calculation (we are not talking about experimental confirmation in the general sense, because not all data of serial TIM are known).

In addition to the calculated mechanical characteristics Fig. 12, 13 provide accompanying dependencies of the TIM start-up parameters, where the stability of active and large changes in reactive resistances are visible.

Usually, to increase the starting torque, designers try to make deep slots in the rotor, so that the increase in the active resistance of its rods works. And it turns out that it is not this that works, but a very significant reduction of

slot scattering due to high strongly saturated rotor teeth, as well as stator teeth.

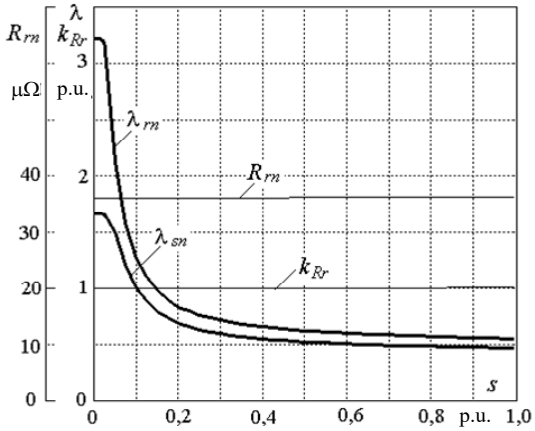

Fig. 12. Active resistance and current displacement coefficient of the rotor rod and magnetic conductivities of the stator and rotor slot scattering as a function of slip

But the influence of the change in the magnetic conductivities of slot scattering on the electromagnetic torque (17) is somewhat smaller, as can be seen from the data in Fig. 12. Because their changes «dissolve» against the background of other more stable active resistances and magnetic conductivities, which are included in (18), (20), (22), (24).

The graphs of the active and reactive resistances of the rotor and stator windings, which are included in (17) as the final values of influence, are given in Fig. 13. And here the undeniable role of reactive resistances and their change in the formation of mechanical characteristics can be seen. But the effect of current displacement, as already mentioned, is practically not manifested, because the active resistance of the phase winding of the rotor R_r' remains practically unchanged.

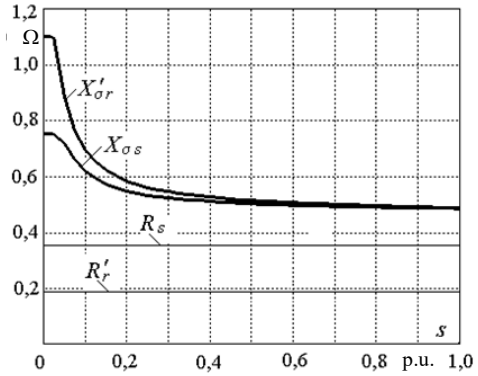

Fig. 13. Active and reactive resistances of TIM windings in the range of changes in slip characteristic of its motor mode of operation

Conclusions.

1. Active and reactive resistances of the windings are important in the TIM design system, but their definition still needs clarification, especially in operating modes with increased slip. Therefore, this problem remains relevant and many theoretical and experimental studies are still devoted to its solution.

2. It was found that for the calculation of the slot scattering fields of the stator and rotor, it is sufficient to use the calculation zone within their tooth pitches with the capture of the slots themselves and adjacent parts of the cores.

3. With unsaturated teeth of the cores, the numerical-field calculation of the magnetic conductivity of slot scattering gave results that exceed the data of classical calculations for rotor slots by 15.7 % and for stator slots by 12.5 %, and for the rotor slot, the main contribution to the error is made by its jumper.

4. Numerical-field calculation of eddy currents in the rotor slot in the same formulation as in classical design, i.e. with unsaturated teeth, nominal current and frequency f_r = 50 Hz gave the current displacement coefficient of 1.35 and an nonuniform distribution of current density with a difference of 2.75 times from the bottom to the top. But when calculating the starting point with real current and strongly saturated teeth, the corresponding values are 1.002 and 1.02, that is, the effect of current displacement is almost absent, contrary to the classics.

5. The method of calculating mechanical characteristics based on the proposed numerical-field approach becomes «transparent» and does not require conditional correction coefficients and reference graphic functions.

6. The calculation of the mechanical characteristics in the slip range from 0 to 1 using the numerical-field method for determining the resistances of the windings, taking into account the corresponding currents in the slots and the saturation of the teeth of the cores, gave results in terms of electromagnetic torque that correspond to the designed and manufactured samples of the TIM, which actually confirms the adequacy of the developed methodology.

7. The analysis showed that when the slip changes, changes in the reactive resistances of the windings have a decisive influence on the shape of the mechanical characteristic and the value of the starting and maximum electromagnetic torques of the TIM, while the active resistances remain practically stable and the effect of current displacement in the rotor slots is almost not manifested, and the main factor is a significant decrease in reactive resistance due to strong saturation of the teeth of the rotor and stator cores.

8. The shown changes in the reactive resistances of the windings are associated with even more pronounced changes in the magnetic conductivities of their slot scattering and, in part, differential scattering. And this is precisely what is affected by the increase in the height of the teeth of the cores, which is associated with an increase in the depth of the slots, but the point is not in the slots and the current squeezed out in them!

9. Thus, the revealed unexpected insignificant effect of current displacement in the squirrel-cage rotor rods on the mechanical characteristics is non-trivial news, and it requires further deeper study and verification on other motors with other shapes and sizes of slots.

Conflict of interest. The author declares no conflict of interest.

REFERENCES

1. Goldberg O.D., Gurin Ya.S., Sviridenko I.S. *Design of electrical machines. 2nd ed., revised and additional*. Moscow, Higher School Publ., 2001. 430 p. (Rus).

2. Kopylov I.P., Goryainov F.A., Klokov B.K. *Electrical machines designing*. Moscow, Yurait Publ., 2011. 767 p. (Rus).
3. Milykh V.I. Numerically-field analysis of the adequacy of the design data of three-phase induction motors and the method of their refinement on this basis. *Technical Electrodynamics*, 2018, no. 1, pp. 47-55. (Rus). doi: https://doi.org/10.15407/techned2018.01.047.
4. Chen H., Bi C. An effective method for determination and characteristic analysis of induction motor parameters. *IET Electric Power Applications*, 2022, vol. 16, no. 5, pp. 605-615. doi: https://doi.org/10.1049/elp2.12180.
5. Ermolaev U., Rudenko T. The definition of asynchronous engines parameters with construction of static characteristics for the milling machine tool СФ-АСТРА-РК8 drives. *Collection of scientific works of KNTU. Machinery in agricultural production, industrial engineering, automation*, 2010, no. 23, pp. 71-77. (Ukr). Available at: http://dspace.kntu.kr.ua/jspui/handle/123456789/1414 (accessed 22 December 2021).
6. Hachicha M.R., Ben Hadj N., Ghariani M., Neji R. Finite element method for induction machine parameters identification. *2012 First International Conference on Renewable Energies and Vehicular Technology*, 2012, pp. 490-496. doi: https://doi.org/10.1109/REVET.2012.6195318.
7. Muteba M., Jimoh A.A. Performance analysis of a three-phase induction motor with double-triple winding layout. *2013 1st International Future Energy Electronics Conference (IFEEC)*, 2013, pp. 131-136. doi: https://doi.org/10.1109/IFEEC.2013.6687492.
8. Yarymbash D.S., Kotsur M.I., Yarymbash S.T., Kotsur I.M. Features of parameter determination of the induction motor substitution circuit for short-circuit mode. *Electrical Engineering and Power Engineering*, 2017, no. 1, pp. 24-30. (Rus). doi: https://doi.org/10.15588/1607-6761-2017-1-4.
9. Tytiuk V., Pozigun O., Chornyi O., Berdai A. Identification of the active resistances of the stator of an induction motor with stator windings dissymmetry. *2017 International Conference on Modern Electrical and Energy Systems (MEES)*, 2017, pp. 48-51. doi: https://doi.org/10.1109/MEES.2017.8248949.
10. Tang J., Yang Y., Blaabjerg F., Chen J., Diao L., Liu Z. Parameter Identification of Inverter-Fed Induction Motors: A Review. *Energies*, 2018, vol. 11, no. 9, art. no. 2194. doi: https://doi.org/10.3390/en11092194.
11. Bednarz S.A., Dybkowski M. Estimation of the Induction Motor Stator and Rotor Resistance Using Active and Reactive Power Based Model Reference Adaptive System Estimator. *Applied Sciences*, 2019, vol. 9, no. 23, art. no. 5145. doi: https://doi.org/10.3390/app9235145.
12. Malyar V.S., Malyar A.V., Andreishyn A.S. A method for calculating mechanical characteristics of induction motors with squirrel-cage rotor. *Electrical Engineering & Electromechanics*, 2019, no. 2, pp. 9-13. doi: https://doi.org/10.20998/2074-272X.2019.2.02.
13. Malyar V.S., Hamola O.Y., Maday V.S., Vasylchyshyn I.I. Mathematical modelling of starting modes of induction motors with squirrel-cage rotor. *Electrical Engineering & Electromechanics*, 2021, no. 2, pp. 9-15. doi: https://doi.org/10.20998/2074-272X.2021.2.02.
14. Dambrauskas K., Vanagas J., Bugenis S., Zimnickas T., Kalvaitis A. Methodology for Asynchronous Motor Impedance Measurement by Using Higher Order Harmonics. *Energies*, 2020, vol. 13, no. 10, art. no. 2541. doi: https://doi.org/10.3390/en13102541.
15. Le Roux P.F., Ngwenyama M.K. Static and Dynamic Simulation of an Induction Motor Using Matlab/Simulink. *Energies*, 2022, vol. 15, no. 10, art. no. 3564. doi: https://doi.org/10.3390/en15103564.
16. *Finite Element Method Magnetics: OldVersions.* FEMM 4.2 11Oct2010 Self-Installing Executable. Available at: http://www.femm.info/wiki/OldVersions (accessed 22 December 2021).
17. Milykh V.I. The system of automated formation of electrical machines computational models for the FEMM software environment. *Technical Electrodynamics*. 2018, no. 4, pp. 74-78. (Ukr). doi: https://doi.org/10.15407/techned2018.04.074.
18. Milykh V.I. Numerical-field analysis of temporal functions and harmonic composition of EMF in windings of a three-phase asynchronous motor. *Technical Electrodynamics*. 2018, no. 3, pp. 56-65. (Rus). doi: https://doi.org/10.15407/techned2018.03.056.

Received 30.08.2022
Accepted 04.11.2022
Published 01.07.2023

V.I. Milykh[1], *Doctor of Technical Science, Professor,*
[1] National Technical University «Kharkiv Polytechnic Institute», 2, Kyrpychova Str., Kharkiv, 61002, Ukraine,
e-mail: mvikemkpi@gmail.com (Corresponding Author)

How to cite this article:
Milykh V.I. Numerical-field analysis of active and reactive winding parameters and mechanical characteristics of a squirrel-cage induction motor. *Electrical Engineering & Electromechanics*, 2023, no. 4, pp. 3-13. doi: https://doi.org/10.20998/2074-272X.2023.4.01